Journal of Aerosol Science 41 (2010) 513–521

Contents lists available at ScienceDirect

Journal of Aerosol Science

journal homepage: www.elsevier.com/locate/jaerosci

Method to measure refractive indices of small nonspherical particles: Application to black carbon particles

Nobuhiro Moteki [a,*], Yutaka Kondo [a], Shin-ichi Nakamura [b]

[a] Research Center for Advanced Science and Technology, University of Tokyo, 4-6-1 Komaba, Meguro-ku, Tokyo 153-8904, Japan
[b] Center for Instrumental Analysis, Aoyama Gakuin University, 5-10-1 Fuchinobe, Sagamihara-shi, Kanagawa 229-8558, Japan

ARTICLE INFO

Article history:
Received 22 December 2009
Received in revised form
23 February 2010
Accepted 23 February 2010

Keywords:
Aerosol optics
Light scattering
Refractive index
Black carbon

ABSTRACT

We demonstrate a new method to measure refractive indices m of small nonspherical particles by simultaneous measurement of particle volume and light-scattering cross section. In contrast to traditional methods, this method can suppress uncertainties due to unknown particle shape. As demonstration of the method, laboratory experiments using an aerosol particle mass analyzer (APM) and single-particle soot photometer (SP2) have been conducted to determine the refractive indices of seven types of commercial black carbon particles and ambient soot at 1064 nm wavelength. Difference in measured $|(m^2-1)/(m^2+2)|$ values among the seven commercial black carbon samples is consistent with the difference in their crystalline structures identified by a transmission electron microscope. The complex refractive index $m=(n, k)$ of ambient soot particles in Tokyo urban area was determined to be $m=(2.26 \pm 0.13, 1.26 \pm 0.13)$.

1. Introduction

Scattering and absorption of light by small particles has long been an important research subject across several disciplines, including atmospheric and oceanic science, astrophysics, bioscience, and medical science. The properties of scattering and absorption are determined by particle volume, shape, and complex refractive index. Refractive indices of bulk matter can be determined by fitting Fresnel's formula onto reflectance and transmittance data of an optically flat surface (e.g., Bohren & Huffman, 1983). For this method, careful preparation of an optically flat surface is critically important to satisfy the applicability condition of Fresnel's formula. The refractive index of fine particulate matter can differ from bulk matter when its production process is gas-to-particle conversion rather than fracturing of parent bulk materials because of structural differences at nanometer scale (e.g., degree of crystallization). Therefore, direct knowledge of the refractive indices of small particles, rather than assuming a value of bulk matter, is desirable for accurate electromagnetic calculations of scattering and absorption by small particles. Measurements of refractive indices of small particles have been made via three distinct approaches: (1) fitting Fresnel's formula to reflectance and transmittance data measured for compressed pellets, (2) fitting Mie theory onto light-scattering data for individual spherical particles, and (3) fitting either Mie theory or some approximation formulas onto scattering and extinction data for particle ensembles. Approach 1 has been used widely to estimate refractive indices of solid aerosols like combustion-generated soot (Mullins & Williams, 1987). However, direct evidence of the optical flatness of pellet surfaces, which is necessary for application of Fresnel's formula, have never been shown for wavelengths shorter than the infrared (Janzen, 1979). Therefore, it would be

* Corresponding author. Tel.: +81 3 5452 5149; fax: +81 3 5452 5148.
E-mail addresses: moteki@atmos.rcast.u-tokyo.ac.jp (N. Moteki), y.kondo@atmos.rcast.u-tokyo.ac.jp (Y. Kondo), snakamura@jm.aoyama.ac.jp (S.-i. Nakamura).

0021-8502/$ - see front matter © 2010 Elsevier Ltd. All rights reserved.
doi:10.1016/j.jaerosci.2010.02.013

difficult to confirm the reliability and reproducibility of the refractive indices derived by approach 1 for visible-to-near infrared wavelengths. In approach 2, measurements of resonance structures in Mie scattering can determine the refractive index with an accuracy of 10^{-5} (Chylek, Ramaswamy, Ashkin, & Dziedzic, 1983). However, this approach is limited only to spherical particles like liquid droplets. In approach 3, the refractive index and size distribution function are simultaneously inferred from extinction or scattering data for an ensemble of particles. Solving this inversion problem requires a theory to connect microphysical and light-scattering properties; Mie theory for spherical particles (Lack et al., 2009) and the Mie theory or Rayleigh–Gans approximation have been used for nonspherical particles (Charalampopoulos, Chang, & Stagg, 1989; Van-Hulle, Talbaut, Weill, & Coppalle, 2002). For polydisperse or nonspherical particles, the inversion results might depend on simplification of the theories (e.g., constraints on the size distribution function, particle-to-particle variation in shape) that have never been a significant concern in previous studies. As mentioned above, although the methods for measuring the refractive indices of small particles are well developed for spherical particles, it still remains a significant issue for nonspherical particles.

In this study, we present a new method for measuring the refractive indices of small particles by simultaneous measurement of the particle volume and scattering cross section. Under ideal conditions, this method does not suffer from artifacts associated with unknown particle shape. In addition, this method enables real-time determination of refractive indices for a very small number of suspended particles, without sample preparation, providing a possible scheme for continuous observation of the refractive indices of aerosols.

Black carbon emitted into the atmosphere from incomplete combustion of fossil fuel and biomass is estimated to be the second strongest contributor to global warming next to carbon dioxide (Ramanathan & Carmichael, 2008). An accurate value of the refractive index of black carbon particles is necessary for quantitative calculation of the efficiency of sunlight absorption. According to a review by Bond and Bergstrom (2006), primary sources of the refractive index of black carbon are limited to less than 20 articles. Among these articles, reported refractive indices for black carbon particles are quite diverse, possibly depending on experimental approach and method of sample preparation. Measurements by the same method are required for accurate comparison of refractive indices of different black carbon particle types. In this paper, a new method to measure refractive index developed here is applied to seven commercially available black carbon samples and ambient soot at 1064 nm wavelength. According to the available databases, it is very likely that refractive indices of black carbon are weakly dependent on or almost independent of wavelength within visible-to-near infrared domain (Chang & Charalampopoulos, 1990; Hess, Koepke, & Schult, 1998; Twitty & Weinman, 1971). Therefore, the accurate measurement only at 1064 nm provided here is significant as a representative of the refractive indices of black carbon in visible-to-near infrared domain.

2. Methods

2.1. Theoretical basis

A fundamental difficulty in solving the problem of scattering by particles is due to the unknown radiation field inside the particle. We have to solve an integral equation to know the internal fields that induce the scattering field (Born & Wolf, 1999). For particles that are optically soft and smaller than the wavelength, the electromagnetic field inside the particle can be approximated by the incident field. By using this approximation, we can simplify the solution of the integral equation to calculate the scattered field. From a mathematical point of view, this approximation corresponds to neglecting higher order (i.e., >1st order) terms of the Neumann series solution of the integral equation (Born & Wolf, 1999). This method is called the first Born approximation or Rayleigh–Gans approximation. The required condition for the Rayleigh–Gans approximation is

$$kd|m-1| \ll 1, \tag{1}$$

where k is the wavenumber, d is the characteristic linear dimension of the particle, and $m=(n, k)$ is its complex refractive index relative to the surrounding medium (Kerker, 1969). A majority of authors (e.g., Bohren & Huffman, 1983; van de Hulst, 1981) require the condition $|m-1| \ll 1|$ in addition to Eq. (1) for the Rayleigh–Gans approximation. Kerker (1969) mentioned that the fundamental requirement of the Rayleigh–Gans approximation is Eq. (1). He only used $|m-1| \ll 1|$ to approximate the final results of the Rayleigh–Gans approximation in simpler form (i.e., $(m^2-1)/(m^2+2) \rightarrow 2(m-1)/3$). Therefore, we shall not always require $|m-1| \ll 1|$ for applicability of the Rayleigh–Gans approximation unless otherwise violating Eq. (1). Under the Rayleigh–Gans approximation, the differential scattering cross section for unpolarized incident light can be written as

$$\frac{dC_{sca}}{d\Omega} = \left|\frac{m^2-1}{m^2+2}\right|^2 v^2 f^2(\Omega, shape, \alpha, \beta, \gamma) \cdot (1+\cos^2\theta). \tag{2}$$

The proportionality constant in Eq. (2) was omitted for simplicity. The Ω is the direction of scattering relative to the incident radiation, v is the particle volume, (α, β, γ) is the Euler angle defining the orientation of the particle, and θ is the scattering angle. The form factor $f(\Omega, shape, \alpha, \beta, \gamma)$ is the amplitude change due to interferences between scattered waves from volume

elements over the entire particle volume defined as

$$f(\Omega,shape,\alpha,\beta,\gamma)=\frac{1}{v}\int_v e^{i\delta}dv=\frac{1}{v}\int_v e^{ik\cdot\Delta d}dv, \tag{3}$$

where δ is the phase shift, k is the wavenumber, and Δd is the change in traveling path of a wave scattered at dv relative to the reference path (van de Hulst, 1981). The reference path is defined as the path of the wave scattered at the coordinate origin and reaching the same observation point. The coordinate origin can be taken at an arbitrary point inside the particle. As the maximum dimension of the particle becomes sufficiently smaller than the wavelength, $|f(\Omega, shape, \alpha, \beta, \gamma)|\to 1$ is independent of the particle shape because $\delta\to 0$ in Eq. (3). The required condition for taking the limit $|f(\Omega, shape, \alpha, \beta, \gamma)|\to 1$ is

$$kd\sin(\theta/2)\ll 1 \tag{4}$$

(van de Hulst, 1981). Under the conditions of Eqs. (1) and (4), the differential scattering cross section per unit squared volume becomes

$$\frac{1}{v^2}\frac{dC_{sca}}{d\Omega}=\left|\frac{m^2-1}{m^2+2}\right|^2(1+\cos^2\theta). \tag{5}$$

The proportionality constant in Eq. (5) was omitted for simplicity. In conclusion, the refractive index of a particle with arbitrary shape can be estimated in the form of Eq. (5) by simultaneous measurements of particle volume and differential scattering cross section under the conditions of Eqs. (1) and (4).

2.2. Implementation of theory to current instruments

In a conventional single-particle optical particle sensor, particles are injected individually into a continuous laser beam and scattered light is collected, detected, and analyzed for particle characterization. For practical purposes, the "differential scattering cross section integrated over the solid angle of light collection $\Delta\Omega$" is defined as the partial scattering cross section ΔC_{sca},

$$\Delta C_{sca}=\int_{\Delta\Omega}\frac{dC_{sca}}{d\Omega}(v,m,shape,\alpha,\beta,\gamma,\Omega)\,d\Omega. \tag{6}$$

The time-dependent signal intensity of scattered light $S(t)$ measured by a photo-detector is proportional to the incident irradiance of laser power $I(t)$ and the partial scattering cross section ΔC_{sca} of the particle,

$$S(t)=I(t)\Delta C_{sca}(t). \tag{7}$$

The proportionality constant in Eq. (7) was omitted. The value $\Delta C_{sca}(t)$ is determined by knowledge of $I(t)$ and measured $S(t)$ with calibration of the proportionality constant in Eq. (7) (Moteki & Kondo, 2008). The ΔC_{sca} is constant over time unless the particles evaporate in the laser beam. Integration of Eq. (5) over $\Delta\Omega$ leads to

$$\frac{\Delta C_{sca}(t)}{v^2(t)}=\left|\frac{m^2-1}{m^2+2}\right|^2 \tag{8}$$

where $v(t)$ is the time-dependent particle volume in the laser beam, which is constant unless the particle evaporates. A proportionality constant in Eq. (8), which has been omitted for simplicity, is determined by calibration using particles with known refractive index and particle volume. With assumption of density, particle volume before evaporation in the laser beam can be estimated by using a currently available instrument to measure particle mass, as demonstrated in the following sections.

2.3. Form factors of nonspherical particles

Correct application of the method requires guidelines for diagnosing applicability of the approximation $|f(\Omega, shape, \alpha, \beta, \gamma)|\to 1$, which is required for the accuracy of relationships Eqs. (5) and (8). To provide such guidelines, we show calculations of the form factor (Eq. (3)) for various size parameters and shapes. The shape of small solid particles formed via gas-to-particle conversion followed by Brownian coagulation can be described by a fractal-like aggregate (e.g., Forrest & Witten, 1979). We calculate form factors for various fractal-like aggregates as representative of a nonspherical particle. We use the particle-cluster aggregation algorithm of Filippov, Zurita, and Rosner (2000) for generation of aggregates of spherical primary particles with specified fractal prefactor k_f, fractal dimension D_f, and number of primaries N. The following relation is satisfied for each aggregate,

$$N=k_f\left(\frac{R_g}{a}\right)^{D_f}, \tag{9}$$

where a is the radius of the primary particle and R_g is the gyration radius defined by coordinate vector $\mathbf{r}_i$ of the i-th primary (i=1, 2, …, N) as

$$R_g^2 = \frac{1}{N}\sum_{i=1}^{N}(\mathbf{r}_i - \mathbf{r}_0)^2, \tag{10}$$

$$\mathbf{r}_0 = \frac{1}{N}\sum_{i=1}^{N}\mathbf{r}_i, \tag{11}$$

(e.g., Filippov et al., 2000). We used k_f=1 for all the calculations. N was varied in the range of 50–1200 depending on particle volume. We define the size parameter (x) for each fractal-like aggregate as the ratio of the circumference of the volume equivalent sphere to the wavelength. The form factor for collection of N-identical scattering elements of random orientation is formulated as

$$|f(\theta)|^2 = \frac{1}{N^2}\sum_{i}^{N}\sum_{j\neq i}^{N}\frac{\sin(hs_{ij})}{hs_{ij}}, \quad \text{where } h = 2k\sin(\theta/2), \tag{12}$$

where s_{ij} is the distance between scattering elements i and j (Kerker, 1969). Eq. (12) was used for calculation of form factors of the fractal-like aggregates, regarding an individual primary particle as a scattering element.

Fig. 1 shows form factors as a function of scattering angle θ for fractal aggregates with (a) D_f=2.8 and (b) D_f=2.0. Results for size parameters $0.3 < x < 0.8$, which cover the range of experiments in this study, are shown. As expected from Eq. (4), $|f(\theta)|^2$ decrease from unity with increasing size parameter. The $|f(\theta)|^2$ also decreases with D_f because of the increase in the typical linear dimension of the particle envelope. As expected from the angular dependence of condition Eq. (4), measuring forward scattering ($0^\circ < \theta < 90^\circ$) is much better than backward scattering ($90^\circ < \theta < 180^\circ$) for suppressing the sensitivity of the form factor to size parameter and particle shape.

3. Experimental

3.1. Hardware

According to the theories in previous sections, simultaneous measurements of ΔC_{sca} and particle volume provide the value $|(m^2-1)/(m^2+2)|$. For this purpose, we use a system connecting a single-particle soot photometer (SP2, Droplet measurement technologies, Inc., USA) (Moteki, Kondo, Takegawa, & Nakamura, 2009; Stephens, Turner, & Sandberg, 2003 and references therein) and an aerosol particle mass analyzer (APM) (Ehara, Hagwood, & Coakley, 1996). The SP2 can monitor the time-dependent $\Delta C_{sca}(t)$ of individual particles in a laser beam (Moteki & Kondo, 2008) at 1064 nm wavelength. The range of scattering angle θ for light collection of the SP2 system was $45 \pm 15^\circ$ and $135 \pm 15^\circ$ (Moteki & Kondo, 2007). The signal acquisition rate of the SP2 was 5 MHz (every 0.2 μs), and ~150 data points of S(t) were taken during particle transit through the laser beam. The lower limit of the size parameter for ΔC_{sca} detection was ~0.3–0.4, corresponding to particle volume of $v = \sim 1 \times 10^{-21}\,\mathrm{m}^3$. The SP2 also measures time-dependent laser-induced incandescence (LII) signals in two visible-bands. As discussed in Section 3.3, we use the LII signals for estimating the time-dependent temperature of a particle in laser beam.

The APM can select aerosol particles by their mass-to-charge ratio by balancing centrifugal and electrostatic forces. The details of the APM instrument used in this study (i.e., APM model 302, KANOMAX, Japan) were described by Moteki and Kondo (2007). The aerosol bipolar charger (^{241}Am) and the APM were connected upstream of the SP2 to measure $\Delta C_{sca}(t)$ of

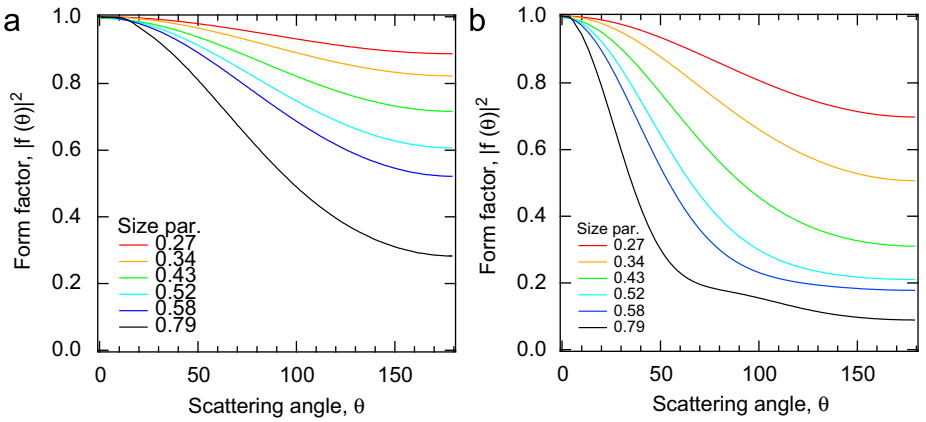

Fig. 1. Calculated form factors $|f(\theta)|^2$ for fractal aggregates with (a) D_f=2.8 and (b) D_f=2.0 as a function of scattering angle. Size parameters are indicated by color as shown in the figure.

known particle mass-to-charge ratio. Singly and multiply charged particles can be discriminated by observing SP2 signals, and only singly charged particles were used for analysis. We need information of the density to determine particle volume from the mass selected by the APM. Uncertainty of the center position of the APM transfer function (center of mass) was estimated to be within 3% from measurements of monodisperse polystyrene latex spheres (JSR Inc., Japan). The width of the APM transfer function was estimated to within $\pm 10\%$ of the center of mass for operating conditions in this study according to numerical simulations of particle trajectories in the APM.

3.2. Black carbon samples

Seven commercially available black carbon samples were measured: fullerene soot (Alfa Aesar, Stock#40971, Lot#FS12S011), colloidal graphite (Alfa Aesar, Stock#41773, Lot#C07M13), Aquadag (Acheson), two types of monodisperse glassy carbon particles with 100- and 50-nm particle diameters (Tokai Carbon, Japan) (Tokai GC-100 nm, 50 nm, respectively), and Aqua-Black 001 and 162 (Tokai Carbon, Japan). We aerosolized these commercial black carbon samples from their water suspensions using a pneumatic nebulizer. The aerosol sample was dried using a diffusion dryer with silica-gels prior to the measurement by the APM-SP2 system. In addition to the seven commercial samples, we also measured ambient soot particles of Tokyo urban area, Japan. The ambient soot particles were extracted from the ambient air by thermal denuding of semi-volatile compounds (i.e., sulfate, nitrate, organics, etc.) with a 400 °C heated inlet (Kondo et al., 2009). After this treatment, these soot samples were directly introduced to the APM-SP2 system. The major source of ambient soot in Tokyo is exhaust of diesel vehicles (Kondo et al., 2006).

The seven commercial black carbon samples were classified into either *graphitic* or *non-graphitic* carbon samples based on their crystalline structures observed by the transmission electron microscope (TEM) images and the electron-diffraction patterns. We used a 400 kV TEM (JEM-4010, JEOL, Inc., Japan) in Aoyama Gakuin University, Japan for these micro-structural analyses. *Non-graphitic* samples showed neither any ordered crystalline structures nor sharp patterns of electron diffraction, indicating that these samples are disordered or amorphous-like carbon in which sp^3 bonds likely present with sp^2 bonds. In contrast, *graphitic* samples showed crystalline structures ordered to some extent and sharp electron-diffraction patterns corresponding to 0.34 nm separations of graphene layers. These evidences indicate that these samples are graphite-like carbon in which the sp^2 bond is dominant. Results of the classification were summarized in Table 1.

Accurate knowledge of density is important for this method, because the relative error in $|(m^2-1)/(m^2+2)|$ value is approximately equal to the relative error in assumed density. According to the manufacturer (Tokai Carbon Inc.), the density of glassy carbon particles is 1.85 g cm^{-3}. Park, Kittelson, Zachariah, and McMurry (2004) reported the density of soot produced from a diesel engine to be 1.77 g cm^{-3}. Mullins and Williams (1987) reported the density of soot particles generated by a diffusion burner with liquid and gas fuel to be 1.77–1.83 g cm^{-3}. Based on the range of reported values, it is likely accurate within 5% to assume the density of non-graphitic carbons as 1.8 g cm^{-3}. In contrast, density of graphite is highly dependent on fraction of internal void, which is likely determined by the extent of ordered graphene structure. The density of graphite materials produced by Alfa Aesar Inc. varies from 1.63–1.80 g cm^{-3} (Alfa Aesar catalogue 2008–2009). These values are significantly less than 1.97–2.26 g cm^{-3}, the range of densities of various graphite powders tabulated by Wissler (2006). In this study, the density of seven commercial black carbon samples and ambient soot were commonly assumed to be 1.8 g cm^{-3} for estimating the particle volume from the mass selected by the APM. Table 1 presents uncertainty of the assumed density (1.8 g cm^{-3}) for graphitic and non-graphitic carbons according to the range of reported values. We assume $\pm 5\%$ uncertainty of the assumed density for ambient soot.

Table 1
Summary of the experimental results.

Sample name	Crystalline structure	Uncertainty in assumed density (1.8 g cm^{-3})	$\Delta C_{sca}/v^2$ value (10^{25} m^{-4}) in plateau regime[a]	$\lvert(m^2-1)/(m^2+2)\rvert$ value[a]	Parameter h[a]
Polystyrene latex sphere	–	–	0.855	0.337	–
Fullerene soot	Non-graphitic	±5%	5.27 (±0.53)	0.84 (±0.04)	0.49 (±0.2)
Colloidal graphite	Graphitic	±25%	11.6 (±5.80)	1.24 (±0.31)	Not determined
Aquadag	Graphitic	±25%	8.30 (±4.15)	1.05 (±0.26)	Not determined
Glassy carbon-100 nm	Non-graphitic	±5%	4.88 (±0.49)	0.81 (±0.04)	0.35 (±0.15)
Glassy carbon-50 nm	Non-graphitic	±5%	5.11 (±0.51)	0.82 (±0.04)	0.43 (±0.18)
Aqua-black 001	Non-graphitic	±5%	3.98 (±0.40)	0.73 (±0.04)	0.08 (±0.1)
Aqua-black 162	Non-graphitic	±5%	4.43 (±0.44)	0.77 (±0.04)	0.21 (±0.13)
Ambient soot	Not available	±5%	4.58 (±0.46)	0.78 (±0.04)	0.26 (±0.13)

[a] The uncertainty due to the assumed density (1.8 g cm^{-3}) was shown in the parenthesis (double-sign corresponds).

3.3. Data analysis

Polystyrene latex spheres (PSLs) (STADEX, JSR, Inc., Japan) with known diameters (152, 202, 294, and 402 nm), density ($1.05\,g\,cm^{-3}$), and refractive index (1.59, 0) were used to calibrate the proportionality constants in Eqs. (7) and (8). The ΔC_{sca} values for the SP2 optical system were calculated by using the Mie scattering code BHMIE (Bohren & Huffman, 1983). At the time of onset of the visible-band LII signals, the particle temperature exceeded 10^3 K, as estimated by the wavelength dependence of the LII signals. It is plausible that a majority of semi-volatile compounds evaporated before this time. As demonstrated by measurements of graphite particles coated by oils (Moteki & Kondo, 2008), evaporation of semi-volatile coatings was estimated to be very small before $t=-2.5\sigma$ of the Gaussian profile under normal operating conditions of the SP2. Therefore, the ratio of the $\Delta C_{sca}(t)$ at $t=-2.5\sigma$ and that just before the onset of the LII signal is an robust indicator of the amount of semi-volatile material coated on refractory black carbon cores. For all black carbon samples, including ambient soot, the mode of histograms of the ratio $\Delta C_{sca}(t=-2.5\sigma)/\Delta C_{sca}(t=\text{onset of LII signal})$ for many particles ranged over 0.9–1.1, depending on the particle species and selection mass. These small systematic deviations of the ratio from 1 demonstrate high purities of black carbon samples used in this study. Particle volume v was estimated from the mass selected by the APM and assumed density of $1.8\,g\,cm^{-3}$. In this study, the $\Delta C_{sca}(t=-2.5\sigma)$ value rather than $\Delta C_{sca}(t=\text{onset of LII signal})$ was used for the $\Delta C_{sca}/v^2$ value, because the particle volume determined by the APM more likely corresponded to $v(t=-2.5\sigma)$ than $v(t=\text{onset of LII signal})$.

To estimate the applicability of the approximation $|f(\theta)|\rightarrow 1$ for our black carbon samples, we present available information on their particle shape and compare this with the calculation results shown in Fig. 1. Fractal dimensions D_f of fullerene soot, Aqua-Black 001, Aqua-Black 162, have been estimated to be larger than $\sim$2.7, the measured relationships between mass and mobility (Moteki et al., 2009). Fractal dimensions of Tokai-GC 50 and 100 nm were estimated as approximately 3 by the same method (unpublished data). From the re-analysis of published data of the mass-to-mobility relationship for ambient soot (Kondo et al., 2006) sampled in the Tokyo urban area in Japan, its fractal dimension was $\sim$2.3. Aquadag and colloidal graphite are a collection of small plate-like fragments (Moteki & Kondo, 2007; Moteki et al., 2009). Therefore, the geometric structure of Aquadag and colloidal graphite are likely more compact than that of a fractal aggregate with D_f=2.0 which is analogous to a plane. Actually, the measured relationships between mass and mobility for Aquadag and colloidal graphite (Moteki & Kondo, 2007; Moteki et al., 2009) indicated the compactness of their particle shapes compared to the ambient soot. Fig. 1b (D_f=2.0) shows that the $|f(\theta)|^2$ is approximately 0.7 averaged over the scattering angles of the SP2 ($\theta=45\pm15^\circ, 135\pm15^\circ$) for the size parameter of 0.3–0.4, corresponding to the particle volume v of the ΔC_{sca} detection limit ($v\sim1\times10^{-21}\,m^3$). Therefore, the $|f(\theta)|^2$ averaged over the SP2 scattering angle for size parameter of 0.3–0.4 is larger than 0.7 provided that the particle shape is more compact than fractal aggregate of D_f=2.0.

As shown in next section, actually measured $\Delta C_{sca}/v^2$ did not systematically decrease with v (i.e., size parameter) for $v<\sim4\times10^{-21}\,m^3$ domain. This indicates that the systematic error due to the decrease of $|f(\theta)|^2$ from 1 with increase in v (i.e., size parameter) is insignificant in the $v<\sim4\times10^{-21}\,m^3$ domain. Practically, we can safely use Eq. (5) assuming $|f(\theta)|^2=1$ after selecting the v domain where the $\Delta C_{sca}/v^2$ becomes almost independent of v.

4. Results and discussion

Measured relationships between $\Delta C_{sca}/v^2$ and v are plotted for all particles in Fig. 2, with Mie calculations of spherical particles with various refractive indices. Each data point and error bar indicates an average and standard deviation for 10^2–10^3 particles. The lower limits of particle volume shown in Fig. 2 correspond to size parameters $x=\sim$0.3–0.4. Within the plateau regime of $\Delta C_{sca}/v^2$, the $\Delta C_{sca}/v^2$ becomes independent of size and shape and depends solely on refractive index. All the data points of PSLs in the 152–402 nm diameter range ($v=1.8\times10^{-21}$–$3.4\times10^{-20}\,m^3$) show close agreement ($<5\%$) with the Mie calculation curve for refractive index (1.59, 0). For PSLs, the $\Delta C_{sca}/v^2$ plateau occurs in the domain $v<\sim1.5\times10^{-20}\,m^3$, corresponding to diameters less than 300 nm or size parameter $x<0.86$. Table 2 summarizes values of $kd|m-1|$ and $kd\sin(\theta/2)$, the left-hand sides of Eqs. (1) and (4), respectively, for various sets of size parameter x and complex refractive index m for the wavelength and scattering angle of the SP2. For x=0.8 and (1.59, 0), $\Delta C_{sca}/v^2$ is within the plateau domain despite neither $kd|m-1|$ nor $kd\sin(\theta/2)$ values being sufficiently smaller than 1. From these experimental facts, the applicability of Eq. (5) can likely be extended with reasonable accuracy to conditions with $kd|m-1|$ and $kd\sin(\theta/2)$ values up to $\sim$1. Black carbon samples show much higher $\Delta C_{sca}/v^2$ values compared to PSLs for the same particle volume, mainly because of their higher $|(m^2-1)/(m^2+2)|$ values than that of PSL. The plateau behaviors can be seen also for a majority of black carbon samples in the small volume regime of $v<1\times10^{-20}\,m^3$. The lower limit of the volumes shown in Fig. 2, v$\sim1\times10^{-21}\,m^3$, corresponds to $x\sim$0.36. From plateau data points with $kd|m-1|$ and $kd\sin(\theta/2)$ values less than $\sim$1, refractive indices can be inferred in terms of the $|(m^2-1)/(m^2+2)|$ value. In this study, we determined the $|(m^2-1)/(m^2+2)|$ value from the average value of measured $\Delta C_{sca}/v^2$ in $v<4\times10^{-21}\,m^3$ domain and summarized in Table 1. Uncertainty of the $|(m^2-1)/(m^2+2)|$ value due to the assumed density is also shown in the table. The $|(m^2-1)/(m^2+2)|$ value showed clear difference between non-graphitic ($|(m^2-1)/(m^2+2)|\sim0.8$) and graphitic ($|(m^2-1)/(m^2+2)|>1$) samples.

Separate determination of the real and imaginary parts of m from the measured $|(m^2-1)/(m^2+2)|$ value requires theoretical or empirical models. In this study, we take an empirical approach as follows. Possible refractive indices take the

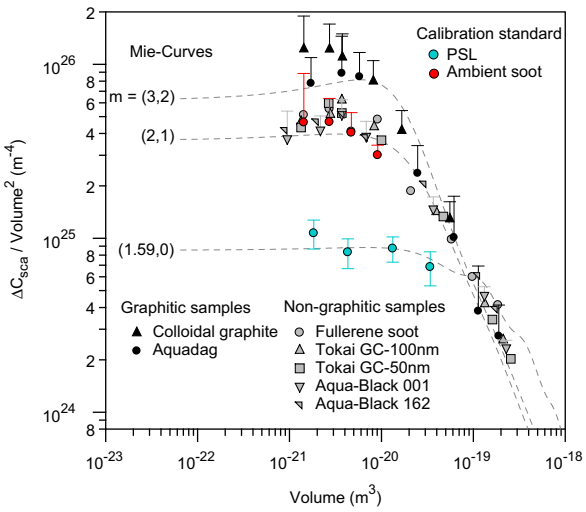

Fig. 2. Measured relationships between the partial scattering cross section divided by the square of particle volume ($\Delta C_{sca}/v^2$) and particle volume (v). Error bars are shown only for several selected species for graphical convenience. Theoretical curves of Mie theory with various complex refractive indices $m=(n, k)$ are also shown.

Table 2
Left-hand sides of Eqs. (1) and (4) for various sets of size parameter and complex refractive index under the given wavelength and scattering angle of the SP2.

Size parameter x, and complex refractive index m	Left-hand side of Eq. (1) $kd\lvert m-1\rvert$	Left-hand side of Eq. (4) $kd\sin(\theta/2)$
0.3, (1.59, 0)	0.35	0.39
0.3, (2.0, 1.0)	0.85	0.39
0.3, (3.0, 2.0)	1.7	0.39
0.8, (1.59, 0)	0.94	1.0
0.8, (2.0, 1.0)	2.3	1.0
0.8, (3.0, 2.0)	4.5	1.0

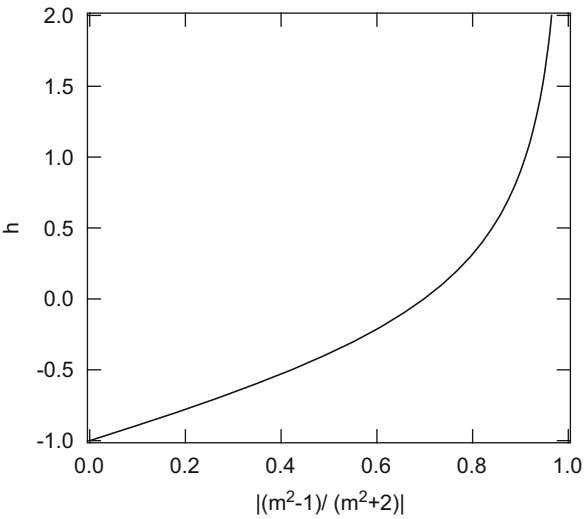

Fig. 3. Calculated relationship between the parameter h and the $|(m^2-1)/(m^2+2)|$ value for the empirical model of complex refractive index $m=(2+h,1+h)$.

values of $m=(n, k)=(2+h, 1+h)$ with h as a parameter. Fig. 3 shows the calculated relationship between the parameter h and $|(m^2-1)/(m^2+2)|$ value for this empirical model. The model can represents the reported values of m of carbon black for visible to near-infrared wavelengths ($m=(2.0, 1.0)$, Janzen, 1979) and that of pure graphite around 1064 nm wavelength ($m=(3.3, 2.1)$, Borghesi & Guizzetti, 1991). This model also fits well the '*void fraction line*' in the n–k plots compiled by Bond

and Bergstrom (2006), the representative relationships between n and k for various black carbon samples at 550 nm wavelength. The parameter h determined from the $|(m^2-1)/(m^2+2)|$ value were summarized in Table 1. Uncertainty of the h value due to the assumed density is also shown in the table. The refractive index of atmospheric black carbon sampled in an urban area (Tokyo, Japan) was determined to be $m=(2.26\pm0.13, 1.26\pm0.13)$. This value is within the range of the m values of five commercial non-graphitic carbon samples (Table 1).

For graphitic carbon samples, we did not show the parameter h in Table 1 because of the h becomes very sensitive to the small error in $|(m^2-1)/(m^2+2)|$ when the $|(m^2-1)/(m^2+2)|$ approaches to 1 as shown in Fig. 3. For graphitic samples, $\Delta C_{sca}/v^2$ data points close to the lower detection limit (i.e., $v<\sim4\times10^{-21}$) are likely still outside the plateau regime, because $kd|m-1|>1$ due to high m values, as expected from the Mie curves in Fig. 2. It is likely that accurate measurements of the $|(m^2-1)/(m^2+2)|$ values for graphitic samples require an extension of the ΔC_{sca} measurement range down to $v=\sim1\times10^{-22}\,\mathrm{m}^3$, in which the $kd|m-1|$ value possibly decreases to less than ~1. Considering the v^2 dependence of ΔC_{sca}, the factor-of-10 extension of the volume range requires a factor-of-100 improvement of the signal-to-noise ratio of ΔC_{sca}. Therefore, this method is less practical for particles with refractive indices much larger than 1.

The relationships between refractive index and crystallographic structure found in this study are consistent with past reports for refractive indices of bulk graphite (3.2, 2.1) (Borghesi & Guizzetti, 1991) and carbon black (2.0, 1.0) (Janzen, 1979), which definitely has less-ordered structure than pure graphite.

5. Summary

We introduced a new method to infer refractive indices of small particles by measuring the relationship between the scattering cross section and particle volume. Because this method is insensitive to particle shape it can be applied to infer refractive indices of highly nonspherical black carbon particles. Particle volumes were estimated from measurements of mass by APM and assumed density. We have inferred refractive indices of eight different black carbon samples at 1064 nm wavelength and demonstrated the consistency between the inferred refractive indices and microphysical structure observed by transmission electron microscope. It was found that the refractive index m of ambient soot sampled in the Tokyo urban area, Japan, was found to be $(2.26\pm0.13, 1.26\pm0.13)$ and similar to the values for other non-graphitic carbon samples. This is a plausible value for the refractive index of ambient soot in urban area and is useful for quantitative improvements in calculations of the climate effects of black carbon.

Acknowledgements

This study was supported by the Ministry of Education, Culture, Sports, Science, and Technology (MEXT), the global environment research fund of the Japanese Ministry of the Environment (B-083), and the Japanese Science and Technology Agency (JST) (SENTAN program).

References

Bohren, C. F., & Huffman, D. R. (1983). *Absorption and scattering of light by small particles*. New York: John Wiley & Sons, Inc.
Bond, T. C., & Bergstrom, R. W. (2006). Light absorption by carbonaceous particles: An investigative review. *Aerosol Science and Technology*, *40*, 27–67.
Borghesi, A., & Guizzetti, G. (1991). Graphite (C). In E. D. Palik (Ed.), *Handbook of optical constants of solids II* (p. 449). New York: Academic Press.
Born, M., & Wolf, E. (1999). *Principles of optics* (7th ed.). Cambridge: Cambridge University Press.
Chang, H., & Charalampopoulos, T. T. (1990). Determination of the wavelength dependence of refractive indices of flame soot. *Proceedings of Royal Society London A*, *430*, 577–591.
Charalampopoulos, T. T., Chang, H., & Stagg, B. (1989). The effects of temperature and composition on complex refractive index of flame soot. *Fuel*, *68*, 1173–1179.
Chylek, P., Ramaswamy, V., Ashkin, A., & Dziedzic, J. M. (1983). Simultaneous determination of refractive index and size of spherical dielectric particles from light scattering data. *Applied Optics*, *22*, 2302–2307.
Ehara, K., Hagwood, C., & Coakley, K. J. (1996). Novel method to classify aerosol particles according to their mass-to-charge ratio-aerosol particle mass analyzer. *Journal of Aerosol Science*, *27*, 217–234.
Filippov, A. V., Zurita, M., & Rosner, D. E. (2000). Fractal-like aggregates: Relation between morphology and physical properties. *Journal of Colloid and Interface Science*, *229*, 261–273.
Forrest, S. R., & Witten, T. A. (1979). Long-range correlations in smoke-particle aggregates. *Journal of Physics A: Mathematical and General*, *12*, L109–L117.
Hess, M., Koepke, P., & Schult, I. (1998). Optical properties of aerosols and clouds: The software package OPAC. *Bulletin of the American Meteorological Society*, *79*, 831–844.
Janzen, J. (1979). The refractive index of colloidal carbon. *Journal of Colloid and Interface Science*, *69*, 436–447.
Kerker, M. (1969). *The scattering of light and other electromagnetic radiation*. New York: Academic Press.
Kondo, Y., Komazaki, Y., Miyazaki, Y., Moteki, N., Takegawa, N. Kodama, D., et al. (2006). Temporal variations of elemental carbon in Tokyo. *Journal of Geophysical Research*, *111*, D12205, doi:10.1029/2005JD006257.
Kondo, Y., Sahu, L., Kuwata, M., Miyazaki, Y., Takegawa, N. Moteki, N., et al. (2009). Stabilization of the filter-based absorption photometry by the use of a heated inlet. *Aerosol Science and Technology*, *43*, 741–756.
Lack, D. A., Cappa, C. D., Cross, E. S., Massoli, P., Ahern, A. T. Davidovits, P., et al. (2009). Absorption enhancement of coated absorbing aerosols: Validation of the photo-acoustic technique for measuring the enhancement. *Aerosol Science and Technologies*, *43*, 1006–1012.
Moteki, N., & Kondo, Y. (2007). Effects of mixing state of black carbon measurement by laser-induced incandescence. *Aerosol Science and Technology*, *41*, 398–417.
Moteki, N., & Kondo, Y. (2008). Method to measure time-dependent scattering cross sections of particles evaporating in a laser beam. *Journal of Aerosol Science*, *39*, 348–364.

Moteki, N., Kondo, Y., Takegawa, N., & Nakamura, S. (2009). Directional dependence of thermal emission from nonspherical carbon particles. *Journal of Aerosol Science*, *40*, 790–801.
Mullins, J., & Williams, A. (1987). The optical properties of soot: A comparison between experimental and theoretical values. *Fuel*, *66*, 277–280.
Park, K., Kittelson, D. B., Zachariah, M. R., & McMurry, P. H. (2004). Measurement of inherent material density of nanoparticle agglomerates. *Journal of Nanoparticle Research*, *6*, 267–272.
Ramanathan, V., & Carmichael, G. (2008). Global and regional climate changes due to black carbon. *Nature Geoscience*, *1*, 221–227.
Stephens, M., Turner, N., & Sandberg, J. (2003). Particle identification by laser-induced incandescence in a solid-state laser cavity. *Applied Optics*, *42*, 3726–3736.
Twitty, J. T., & Weinman, J. A. (1971). Radiative properties of carbonaceous aerosols. *Journal of Applied Meteorology*, *10*, 725–731.
van de Hulst, H. C. (1981). *Light scattering by small particles*. New York: Dover.
Van-Hulle, P., Talbaut, M., Weill, M., & Coppalle, A. (2002). Inversion method and experiment to determine the soot refractive index: application to turbulent diffusion flames. *Measurement Science and Technology*, *13*, 375–382.
Wissler, M. (2006). Graphite and carbon powders for electrochemical applications. *Journal of Powder Sources*, *156*, 142–150.